

# Forcing Boundary-Layer Transition on an Inverted Airfoil in Ground Effect

L S Roberts<sup>a</sup>, M V Finnis<sup>b</sup>, K Knowles<sup>c</sup> and N J Lawson<sup>d</sup>  
*Cranfield University, UK*

The influence of the laminar boundary-layer state on a wing operating in ground effect has been investigated using experiments with a model that provides two-dimensional flow. The effect of a boundary-layer trip placed at varying distances from the leading edge was observed at various incidences in terms of on-surface characteristics, including pressure measurements, flow visualisation and hot-film anemometry, and off-surface characteristics with velocity surveys below and behind the wing. The act of forcing transition led to downforce being reduced and drag increased, moreover it altered almost all aspects of the wing's aerodynamic characteristics, with the effect becoming greater as the trip was placed closer to the leading edge. These aspects include the replacement of a laminar separation bubble with trailing-edge separation, a thicker boundary layer, and a thicker wake with greater velocity deficit. The importance of considering laminar phenomena for wings operating in ground effect has been shown.

## Nomenclature

$c$	Wing chord length, m
$C_D$	Drag coefficient
$C_F$	Friction coefficient

<sup>a</sup> PhD Researcher, Aeromechanical Systems Group, Centre for Defence Engineering

<sup>b</sup> Principal Research Fellow, Aeromechanical Systems Group, Centre for Defence Engineering

<sup>c</sup> Professor of Aeromechanical Systems, Aeromechanical Systems Group, Centre for Defence Engineering,

Defence Academy of the United Kingdom, Shrivenham, SN6 8LA

<sup>d</sup> Professor of Aerodynamics and Airborne Measurement, National Flying Laboratory Centre

$-C_L$	Downforce coefficient
$C_P$	Pressure coefficient
CV	Coefficient of variation of quasi-shear stress
$E$	Hot-film output voltage, V
$E_0$	Hot-film zero voltage, V
$f$	Frequency, Hz
$h$	Ground clearance, m
$M$	Mach number
$N$	Critical amplification factor
PSD	Power spectral density, $(\text{Nm}^{-2})^2$
$Re_c$	Chord-based Reynolds number $(\frac{Vc}{\nu})$
$Re_\theta$	Momentum-thickness Reynolds number $(\frac{V\theta}{\nu})$
$V$	Freestream flow velocity, $\text{ms}^{-1}$
$x, y, z$	Cartesian coordinates, origin at leading edge, m
$\Delta W_A$	Percentage difference in the area bounded by velocity deficit, % $(\frac{W_{A-Forced} - W_{A-Free}}{0.5(W_{A-Forced} + W_{A-Free})})$
$\alpha$	Incidence, $^\circ$
$\delta^*$	Displacement thickness, m
$\theta$	Momentum thickness, m
$\nu$	Kinematic viscosity, $\text{m}^2\text{s}^{-1}$
$\sigma$	Standard deviation of quasi-wall-shear stress, $\text{Nm}^{-2}$
$\tau_Q$	Quasi-wall-shear stress $(\frac{E^2 - E_0^2}{E_0^2})^3$ , $\text{Nm}^{-2}$
$\overline{\tau_Q}$	Mean quasi-wall-shear stress, $\text{Nm}^{-2}$

## I. Introduction

### A. Background

Wings in ground effect have long been studied from the perspective of aircraft performance during take-off and landing or ground-effect machine design [1–9]. These are all cases where the wing generates lift upwards (i.e. away from the ground). More recently wing-in-ground-effect studies

have been extended to include down-lifting wings [10–15], which are relevant to aircraft (low-set) tailplanes during take-off rotation or motorsport applications.

## B. Flow Phenomena

It has been comprehensively shown that as the distance between an inverted wing and the ground decreases the wing will generate more downforce as flow is constrained between it and the ground, hence increasing suction levels [10–15]; this is termed the force-enhancement region. This phenomenon holds true until the ground clearance reduces to a critical value, beyond which the flow can no longer overcome the adverse pressure gradient associated with the increased suction levels, and thus the boundary layer separates; this is denoted the force-reduction region. Correia et al. [15] found that at  $Re_c = 1.63 \times 10^5$  the force-reduction region could also be associated with the de-cambering of the wing’s effective shape, as a result of the separation bubble that formed on the suction surface becoming increasingly smaller, and thus reducing its influence on the wing, as the ground clearance reduced. A laminar separation bubble was also noted by Zerihan & Zhang [13] to be the transition mechanism for an inverted wing in ground effect operating at  $Re_c = 4.67 \times 10^5$ , although no further investigation of the bubble was conducted.

## C. Reynolds Number Ranges of Interest

Despite this body of existing work there has been little discussion of the effect of Reynolds number and boundary layer transition on the performance of wings in ground effect. Many of the applications of interest for down-lifting wings in ground effect, however, feature low Reynolds numbers because of the small size and low speeds involved (particularly by comparison with aircraft main-plane chords and cruise speeds). A Reynolds number range of  $4 \times 10^5 \leq Re_c \leq 1.2 \times 10^6$  is equivalent to a light aircraft tail during its take-off run, when the tailplane is used to raise the nose. For example, a Cessna 172 has a tailplane chord of approximately 0.58 m and a take-off speed of approximately  $100 \text{ km hr}^{-1}$ , giving  $Re_c = 1.1 \times 10^6$ . For an aircraft with a lower take-off speed and smaller tailplane, such as a glider, this could be down to  $Re_c = 6 \times 10^5$  and for a small UAV using a ground-roll take-off it is as low as  $Re_c = 2.2 \times 10^5$ . By comparison, a racing car will operate over a speed range of 70-300  $\text{km hr}^{-1}$ , equating to a Reynolds number range of approximately

$3.2 \times 10^5 \leq Re_c \leq 1.35 \times 10^6$ , based on the front wing main-plane chord.

#### **D. Boundary-Layer Tripping**

Zerihan & Zhang [13] and Correia et al. [15] both conducted tests in which boundary-layer trips were used to force the boundary layer to transition to a turbulent state. Zerihan & Zhang [13] observed a loss of maximum downforce coefficient from  $C_L = 1.72$  to  $C_L = 1.15$  when a roughness-type trip was placed at  $x/c = 0.1$  on the suction surface of a Tyrrell-026 wing. Surface pressure measurements showed that this was due to a reduction in both suction and pressure on their respective surfaces, and trailing-edge separation increasing in the forced-transition case. The authors cited a thicker boundary layer encountering the adverse pressure gradient as being the cause of this increase in trailing-edge separation. Correia et al. [15] also used a roughness-type trip placed at  $x/c = 0.25$  on the suction surface of a GA(W)-1 profile, in which a reduction in downforce was similarly observed. The authors cited the elimination of the separation bubble as a mechanism for de-cambering the effective shape of the wing, such that circulation was diminished.

#### **E. Fully-Turbulent Modelling**

Although there have been numerous studies on inverted wings operating in ground effect, at relatively low Reynolds numbers, the aspects of laminar boundary layers and boundary-layer transition are often over-looked. Even the most recent computational studies [16, 17] have made use of fully-turbulent closure models despite operating at a Reynolds number at which transitional phenomena are still prevalent and, in the case of the latter study, observing the effect of Reynolds number scaling. Despite the low Reynolds number conditions of each of these studies, none has included laminar phenomena. Moreover, computations by Zerihan & Zhang [18] and Doig et al. [19] both used forced-transition experimental results when comparing to their fully-turbulent models, showing that laminar effects were clearly manifesting in the experimental results.

#### **F. Aims & Objectives**

The present study intends to confirm the existence of a laminar separation bubble at a Reynolds number applicable to a light aircraft's tailplane during take-off or a full-scale racing car on track. It will investigate the influence of the laminar boundary layer on the aerodynamic characteristics of

the aerofoil by forcing transition to a turbulent state with roughness-type trips at various chordwise locations. This will allow the assumption of using fully-turbulent closure models for computational analysis to be evaluated, and also provide further insight into the practise of forcing transition for wind-tunnel testing of wings operating in ground effect.

## II. Description of Study

Experiments were conducted in the DS Houghton wind tunnel at the Defence Academy of the United Kingdom, in Shrivenham, UK. This is a 2.8 m  $\times$  1.8 m closed-return, three-quarter-open test section wind tunnel equipped with a continuous-belt rolling road. The belt speed is automatically synchronized with the freestream velocity by the wind tunnel control system. The boundary-layer on the road is removed through boundary-layer suction applied through perforated plates ahead of a knife-edge transition to the road. Further information on this tunnel is given by Knowles & Finnis [20].

The DS Houghton wind tunnel is large enough to contain 50% scale racing-car models, however, for these models the maximum chord-based Reynolds number which can be attained is limited to approximately  $Re_c = 2.8 \times 10^5$ . In order to investigate higher Reynolds number flows a two-dimensional study was conducted so that a super-scale model (150%), which allowed more relevant Reynolds numbers to be achieved, could be implemented. A computer-generated model of the experimental setup inside the DS Houghton wind tunnel is given in Fig. 1. All tests were conducted at a ground clearance of  $h/c = 0.3$  and a chord-based Reynolds number of  $Re_c = 6 \times 10^5$ .

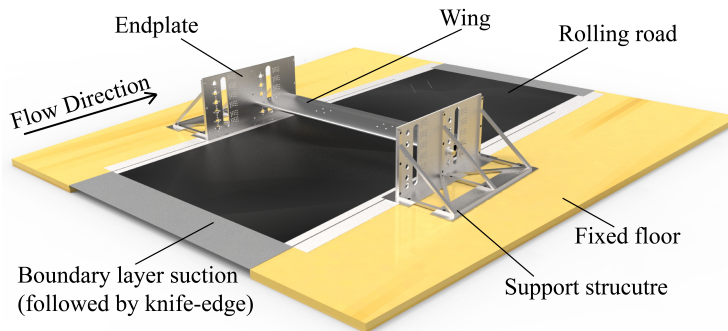


Fig. 1 Drawing of experimental setup

## A. Test Model

The wing is an untapered, untwisted, constant-section GA(W)-1 aerofoil section wing of aspect ratio 5.14 and chord 350 mm. The wing consists of three hollow sections each of span 570 mm, each of which is purpose-designed for a specific experimental technique and which can be re-arranged in any order; the active section for measurement was always placed in the middle. One section has static pressure tappings in the suction surface, one has hot-film gauges set into the suction surface, and one is clean such that flow-visualisation paint can be applied to it. Each wing section comprises of two parts, an upper and a lower section, so that the instrumentation can be accessed. The upper section is essentially inserted into the lower section; this means that the joins between the two sections are confined to the upper (pressure) surface and thus have minimal effect on flow across the suction surface, where all measurements are taken.

The wing is mounted from two endplates, which allow for ground clearance and incidence changes, that are mounted either side of the rolling road. Incidence is altered by rotating the wing around a brass pin located at  $x/c = 0.25$ . As the incidence is altered the ground clearance, which is defined as the distance between the lowest point on the wing's surface and the ground, alters by  $h/c = 0.012$  and  $h/c = 0.017$  in the  $\alpha = 3^\circ$  and  $\alpha = 5^\circ$  cases respectively. To ensure that the wing was not being disturbed by vibrations, due to either the rolling road or wind-tunnel fan, a 6-axis accelerometer was fixed inside the wing at  $x/c = 0.5$ . Some low-energy frequencies at around 500 Hz were observed, however these were deemed of sufficiently high frequency that their influence on the low-speed flow was negligible. Measurements taken during the setup of the wing in the tunnel showed that it was oriented at  $0.008^\circ \pm 0.0013^\circ$  in roll,  $0^\circ \pm 0.033^\circ$  in yaw, and  $(\alpha + 0.054^\circ) \pm 0.022^\circ$  in incidence.

The finite aspect ratio of the wing means that the flow will never be truly two-dimensional. The two-dimensionality of the flow was investigated using wool tufts, which showed that flow remained in the streamwise direction in the central section and no regions of large separation or high turbulence were present on the wing. An additional test involved using a traverse-mounted Pitot tube, which rested on top of the wing to keep it stable, to measure the spanwise pressure gradient across the wing. The results showed that the dynamic pressure varied by 0.7 Pa across the entire central

section of the wing (570 mm), when only the span at which measurements are taken is considered, the variation is only 0.12 Pa. Moreover, the total pressure varied by 0.45 Pa across the 570 mm span of the central section. Based on the results of these two tests, the flow in the region where measurements are taken can be considered acceptably two-dimensional.

#### **B. Pressure Measurements**

Static pressure measurements were taken through thirty-one tappings in the suction surface at equal spacing from  $x/c = 0.1$  to  $x/c = 0.85$ . The tappings were placed in two diagonal lines so that the interaction between consecutive tappings was kept to a minimum; all tappings were located within  $z/c = 0.14$  of the wind tunnel centreline. The pressure was recorded by a 0 – 10 "W pressure transducer at 2 kHz, with a 1 kHz filter, for 20 secs at each tapping consecutively. The freestream flow conditions were logged simultaneously with each individual tapping; these readings ensured that the normalised pressure coefficient was accurately computed for each tapping.

#### **C. Flow Visualisation**

Flow visualisation was conducted using a paint consisting of paraffin, oleic acid and fluorescent pigment. The paint was applied prior to running using a spray bottle, the tunnel was then run for 30 minutes to allow the paraffin to evaporate. Once the wind had stopped the wing was rotated upwards and photographs taken under ultra-violet light. The post-processing of these photographs involved using an 8-bit gray-scale followed by a histogram equalisation, this method improves the contrast between streaklines to make them more defined.

#### **D. Hot-Film Anemometry**

Nine Dantec 'Glue-on' hot-film gauges were set into the suction surface, such that they were flush with the surface, at equal streamwise spacing from  $x/c = 0.45$  to  $x/c = 0.85$  at intervals of  $x/c = 0.05$ . Similarly to the pressure tappings, the hot-film gauges were set in a diagonal line so that the interaction between gauges would be minimal. The output of all nine gauges was recorded simultaneously at a frequency of 2 kHz, with a 1 kHz anti-aliasing filter, for a total of 98 seconds. Wind-off data were recorded both before and after each run.

The hot-film gauges were uncalibrated, so only semi-quantitative information could be gathered.

Zhang et al. [21] evaluated the hot-film data as quasi-wall-shear stress ( $\tau_Q$ , Eqn. 1). The coefficient of variation (CV, Eqn. 2) is used to indicate boundary-layer state. In the laminar state CV is low because the flow is steady, whereas CV is higher in the turbulent boundary layer because of the velocity fluctuations that characterise turbulent flow. A sharp rise in the variance was used to determine the point of boundary-layer transition. It should be noted, however, that a high value of CV can also be the result of a low mean as well as of a high standard deviation. Zhang et al. [21] used normalised RMS to characterise the boundary-layer state. However, it appears that their RMS is of an AC coupled value and hence their normalised RMS is equivalent to CV.

Given that the coefficient of variation of the hot-film data can be used as an indication of turbulence, the standard error for each gauge in each case is different. Gauges positioned in the turbulent boundary layer will inherently have a larger uncertainty as a result of the larger coefficient of variation.

$$\tau_Q = \left( \frac{E^2 - E_0^2}{E_0^2} \right)^3 \quad (1)$$

$$CV = \frac{\sigma}{\bar{\tau}_Q} \quad (2)$$

The time history of each hot-film gauge was converted to  $\tau_Q$  point by point, using  $E_0$  obtained by averaging values before and after running the tunnel, and then transformed into a PSD by averaging spectra calculated from 1.024 sec lengths (2048 points).

### E. LDA Measurements

Laser Doppler anemometry (LDA) was conducted in the wake at  $x/c = 1.5$ ,  $x/c = 2$  and  $x/c = 3$ , as well as underneath the wing at  $x/c = 0.375$ , using a two-component 0.7 W TSI system. Each measurement survey contained between 40 and 50 grid points at 1 – 4 mm spacing, where smaller spacing was used in regions of significant velocity gradient. Each grid point was formed of a total of 10,000 samples that were recorded at approximately 600 Hz. Seeding was introduced into the diffuser of the closed-return wind tunnel with a TSI six-jet atomiser. Whilst the other measurements used a



constant Reynolds-number mode, this could not be used for the LDA measurements as measurement of the freestream velocity could not be synchronized with each data point, and thus allowing the tunnel to alter the velocity would have skewed the results. The uncertainty of each data point is dependent on the turbulence stresses, whereby the higher the stress the greater the uncertainty. The maximum uncertainty in the measured velocity at any data point was found to be  $\pm 0.027 \text{ ms}^{-1}$  at a 95% confidence level; this data point was that which occurred at the centre of the wake, where the highest turbulent stress occurred. Outside the wake the uncertainty reduced to  $\pm 0.0039 \text{ ms}^{-1}$ .

In order to place the LDA measurement volume close to the wing, only the x-component of velocity could be measured. The vertical component was also recorded, however, in order to ascertain the actual flow direction to ensure that it was an acceptable approach to observe only the single component. It was found that the flow angle was  $0.76^\circ$  at  $\alpha = 0^\circ$ , and  $1.78^\circ$  at  $\alpha = 5^\circ$ .

#### **F. Forced-Transition Tests**

Forced-transition tests were conducted using roughness-type trips of streamwise length  $x/c = 0.05$  placed on the suction surface at varying distances from the leading edge to an accuracy of  $\pm 0.0014c$ , where the leading edge of the trip is considered to be the datum line. Forcing transition requires that the boundary-layer momentum thickness be increased by inducing perturbations in the flow. In this case this is completed by using a strip of very rough material. As such, trips were made from a double-sided tape covered, on one side, with grit of size  $265 \mu\text{m}$  (grit 60). This gave a total trip height of  $0.415 \text{ mm}$ .

### **III. Results**

#### **A. Pressure Measurements**

The static pressure distribution for the suction surface of the wing at varying incidence  $0^\circ \leq \alpha \leq 5^\circ$  is given in Fig. 2; it should be noted that the tappings covered by the trips have been removed. In addition to the free-transition case, forced-transition tests were conducted with the trip placed at  $x/c = 0.1, 0.3, 0.5$ . At  $\alpha = 0^\circ$  the free-transition exhibits a laminar separation bubble of significant size, in the region approx.  $0.6 \leq x/c \leq 0.8$ , such that it has a considerable effect on the pressure distribution. The separation bubble alters the effective shape of the wing, leading

to a region of constant pressure being produced. As incidence is increased to  $\alpha = 3^\circ$  the point of maximum suction moves upstream beyond  $x/c = 0.1$ , and the magnitude of suction increases. Despite the stronger adverse pressure gradient, the presence of a laminar separation bubble can still be observed at approx.  $0.55 \leq x/c \leq 0.75$ . Increasing the incidence further to  $\alpha = 5^\circ$  causes the magnitude of suction to increase again, however no evidence of a separation bubble can be observed in the pressure distribution for  $\alpha = 5^\circ$ .

For forced-transition tests some tappings were blocked by the trip, the readings from these tappings have been removed from Fig. 2. It can be observed, however, that the trip does still have an effect on the other tappings immediately either side of it. This is a result of the physical size of the trip, which causes a stagnation on its leading edge and slows the flow slightly such that both tappings before and after the trip exhibit slightly lower suction than the general trend of the distribution would otherwise suggest. This was somewhat unavoidable, however, because it was not possible to alter the surface roughness at varying points without placing an object on the wing's surface.

In all cases the boundary layer is tripped prior to the free-transition laminar separation point ( $x/c \approx 0.6$ ). The presence of the turbulent boundary layer in the adverse pressure gradient means that the laminar separation bubble does not occur. With transition forced at  $x/c = 0.1$  a turbulent boundary layer covers the majority of the wing, which leads the magnitude of suction across the entire chord to be dramatically reduced, with the maximum suction value that occurs at  $x/c = 0.45$

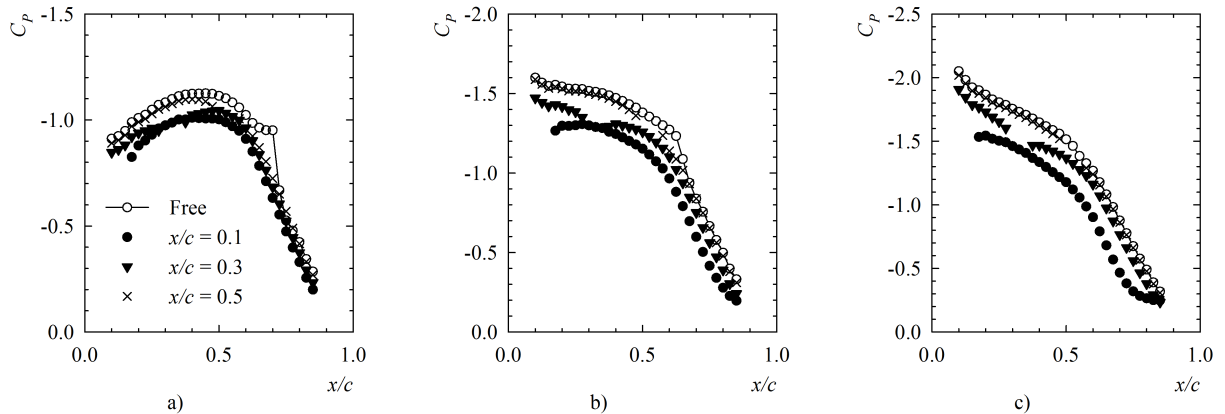


**Fig. 2** Suction-surface pressure distribution at a)  $\alpha = 0^\circ$ , b)  $\alpha = 3^\circ$ , and c)  $\alpha = 5^\circ$

being reduced by 10.5%. Moving the trip downstream to  $x/c = 0.3$  leads to a pressure distribution that is similar to that of the  $x/c = 0.1$  trip case, however the magnitude of suction is slightly increased. The same trend holds true by moving the trip to the most downstream location of  $x/c = 0.5$ ; at which the magnitude of suction is very similar to that of the free-transition, the only difference being the lack of the constant-pressure region due to the removal of the separation bubble.

As the incidence is increased from  $\alpha = 0^\circ$  to  $\alpha = 3^\circ$  and finally on to  $\alpha = 5^\circ$  the same trends hold true, in that as the trip is moved upstream the magnitude of suction is progressively reduced, thus the downforce being produced by the wing is incrementally reducing. Moreover, as incidence is increased the magnitude of suction loss also increases. At  $\alpha = 5^\circ$  for the  $x/c = 0.1$  forced-transition case the pressure distribution indicates that trailing-edge separation is occurring, further reducing downforce.

As the incidence is increased the influence of the laminar separation bubble becomes less prominent, which leads to the  $x/c = 0.5$  trip more closely representing the free-transition static pressure distribution. The earlier transition location and lack of separation bubble exhibited by the  $\alpha = 5^\circ$  incidence case leads to a transition location for the free-transition case and the forced-transition location of  $x/c = 0.5$  becoming similar.

Selig, et al. [22] tested 34 airfoil sections and concluded that the laminar separation bubble dominated the performance of the airfoil at Reynolds numbers  $8 \times 10^4$  to  $1 \times 10^5$ . It has been shown, however, in the present work that even at  $Re_c = 6 \times 10^5$  the separation bubble can still have a significant influence on the airfoil.

## B. Flow Visualisation

The suction-surface flow visualisation is presented in Fig. 3 for various incidences. In free-transition at  $\alpha = 0^\circ$  and  $\alpha = 3^\circ$  the presence of the laminar separation bubble can be observed; as incidence is increased the bubble moves upstream as a result of the stronger adverse pressure gradient. The streaklines before and after the bubble can therefore be observed as occurring in the laminar and turbulent boundary-layer states respectively. For  $\alpha = 5^\circ$ , however, the flow clearly remains attached until very close to the trailing edge. The location of transition can still be inferred from the streaklines observed at  $x/c \approx 0.45$ , as prior to this region the streaklines are similar to the

laminar state of the  $\alpha = 0^\circ$  and  $\alpha = 3^\circ$  cases, and downstream of this region they are similar to those observed in the turbulent region of the  $\alpha = 0^\circ$  and  $\alpha = 3^\circ$  cases. Moreover, the whiter and thicker nature of the streaklines at  $x/c \approx 0.45$  for the  $\alpha = 5^\circ$  case indicates that the shear stress is quite low; it then quickly transforms to a darker shade, which suggests that shear stress has risen. A rise in shear stress would indicate the start of a turbulent boundary layer, so again showing that this is the region of transition.

The act of forcing transition eliminates the formation of the laminar separation bubble as the turbulent boundary layer is more resilient to the adverse pressure gradient. Despite this, trailing-edge separation occurs for the forced-transition cases by varying amounts; where the  $x/c = 0.1$  trip causes the boundary layer to separate earlier. For  $\alpha = 0^\circ$  the separation point is downstream of  $x/c = 0.85$ , hence it was not observed in the static pressure measurements.

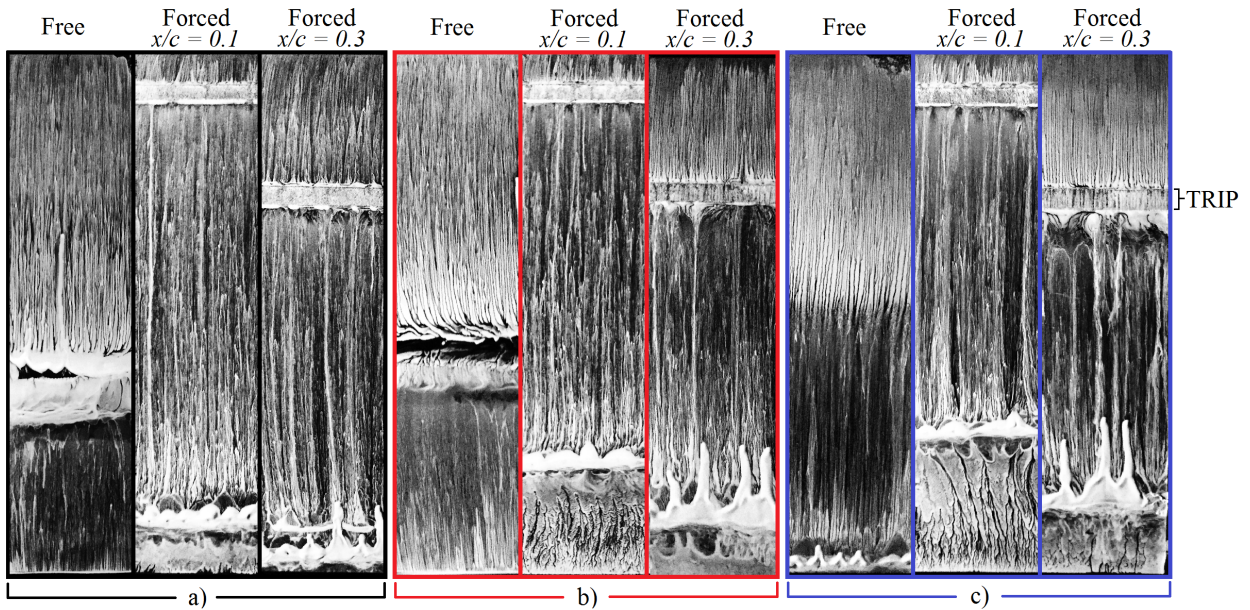


**Fig. 3** Flow visualisation at a)  $\alpha = 0^\circ$ , b)  $\alpha = 3^\circ$ , and c)  $\alpha = 5^\circ$  (Flow moving top to bottom)

Trailing-edge separation is the result of two aspects: firstly, the laminar separation bubble has the effect of re-energising the boundary layer part-way through the pressure recovery, thus helping it overcome the adverse pressure gradient. Secondly, momentum loss in a turbulent boundary layer is greater than in a laminar boundary layer due to the fluctuating velocity components, so when the turbulent boundary layer is forced to begin at an earlier position, the momentum lost by a

given downstream location is greater. Thus for the  $x/c = 0.1$  case trailing-edge separation occurs earliest. The result of trailing-edge separation is the reduced suction observed in the static pressure measurements as circulation is reduced. Thus the decreasing suction magnitude when moving the trip upstream observed in the previous section, is a result of the trailing-edge separation point moving upstream.

For all tested incidences, the same trends are observed. Although no laminar separation bubble was observed for the  $\alpha = 5^\circ$  case, the large trailing-edge separation that occurs shows that the momentum loss is arguably a more important aspect than the re-energising mechanism of the separation bubble. It was observed in the previous section that the reduction in suction of the forced-transition cases becomes greater as incidence is increased. It can be observed from Fig. 3 that this is due to the forced-transition cases exhibiting increasingly earlier trailing-edge separation points as incidence is increased. This is because as the adverse pressure gradient becomes stronger the momentum loss in the turbulent boundary layer increases. Forcing transition at  $x/c = 0.5$  for incidence  $\alpha = 5^\circ$  showed an almost identical pressure distribution to the free-transition case, which is clearly a result of the laminar and turbulent boundary-layer portions being of equal length in this forced case and in the free-transition case.

### C. Hot-Film

The quasi-shear-stress distribution shown in Fig. 4 and coefficient of variation shown in Fig. 5 allow the boundary-layer separation, transition and reattachment points to be investigated further. Although the spatial resolution of the hot-film gauges is not enough to give precise locations of these phenomena, it is adequate to compare different cases. The quasi-shear-stress distribution allows regions of separation to be found, as the shear stress in such regions is zero. The coefficient of variation is primarily used to determine the state of the boundary layer; under the laminar boundary layer the CV is small due to the steady orderly flow, whilst the turbulent boundary layer exhibits large CV due to the eddies of varying spatial and temporal scales that it contains. Hence a rise in CV depicts the transition to a turbulent state.

Fig. 4 shows that in free transition a laminar separation bubble, as shown by the region of zero shear stress, occurs for  $\alpha = 0^\circ$  at approximately  $0.6 \leq x/c \leq 0.7$  and for  $\alpha = 3^\circ$  at approximately

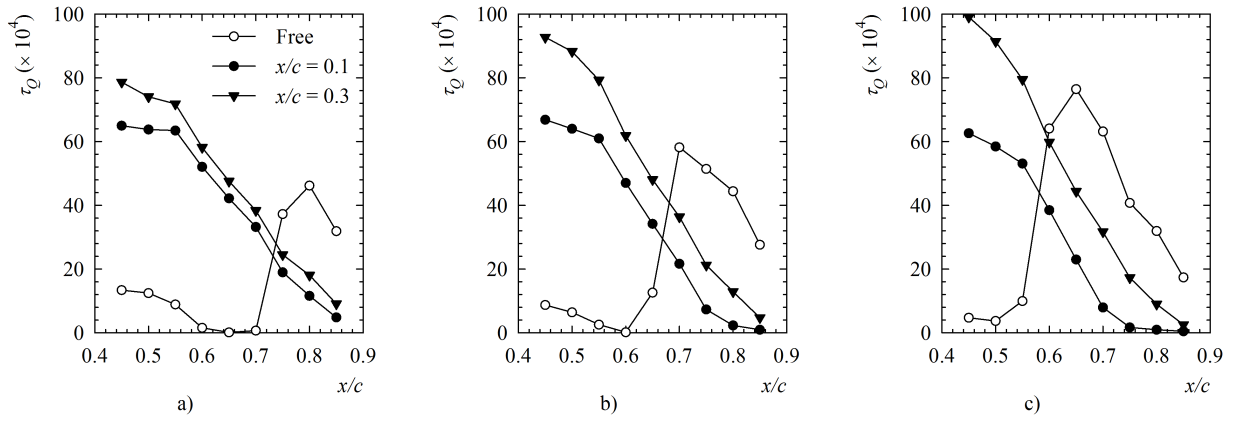


**Fig. 4** Quasi-wall-shear stress for free- and forced-transition cases at incidence a)  $\alpha = 0^\circ$ , b)  $\alpha = 3^\circ$ , and c)  $\alpha = 5^\circ$  ( $Re_c = 6 \times 10^5$ )

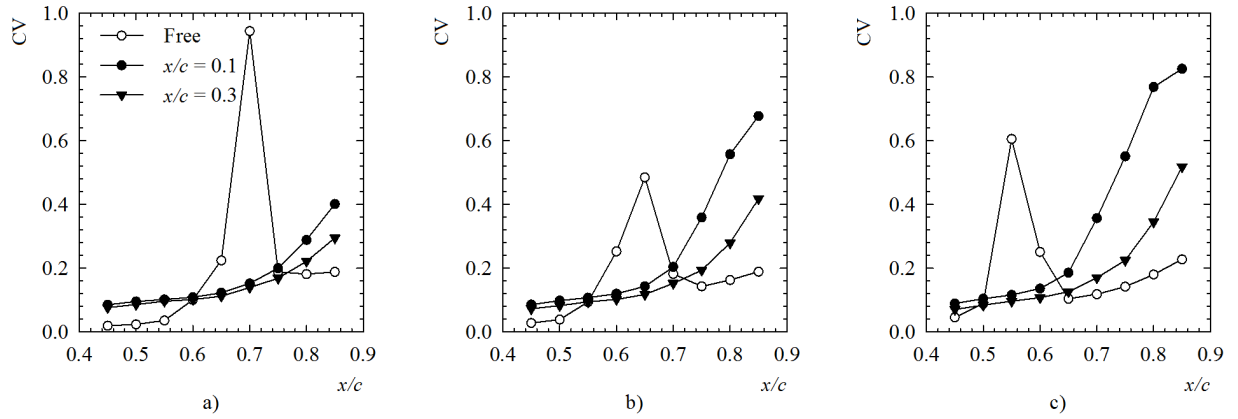


**Fig. 5** Coefficient of variation for free- and forced-transition cases at incidence a)  $\alpha = 0^\circ$ , b)  $\alpha = 3^\circ$ , and c)  $\alpha = 5^\circ$  ( $Re_c = 6 \times 10^5$ )

$x/c = 0.6$ ; showing that the bubble has moved upstream and also become shorter in length. For  $\alpha = 5^\circ$  no region of zero shear stress is observed prior to the rise in shear stress that is synonymous with the transition to a turbulent state. Hence it must be concluded that transition has occurred in the attached boundary layer. The coefficient of variation, given in Fig. 5, shows that the rise in CV, which demonstrates turbulence, occurs at the location prior to reattachment of the boundary layer for  $\alpha = 0^\circ$ ; this is because turbulence is generated in the separated shear layer first, and then the boundary layer reattaches. The most important observation of the free-transition case for Fig. 5, however, is the difference between the laminar and turbulence boundary-layer state signals. Based on this observation, it can be stated that a turbulent boundary layer has been formed in the

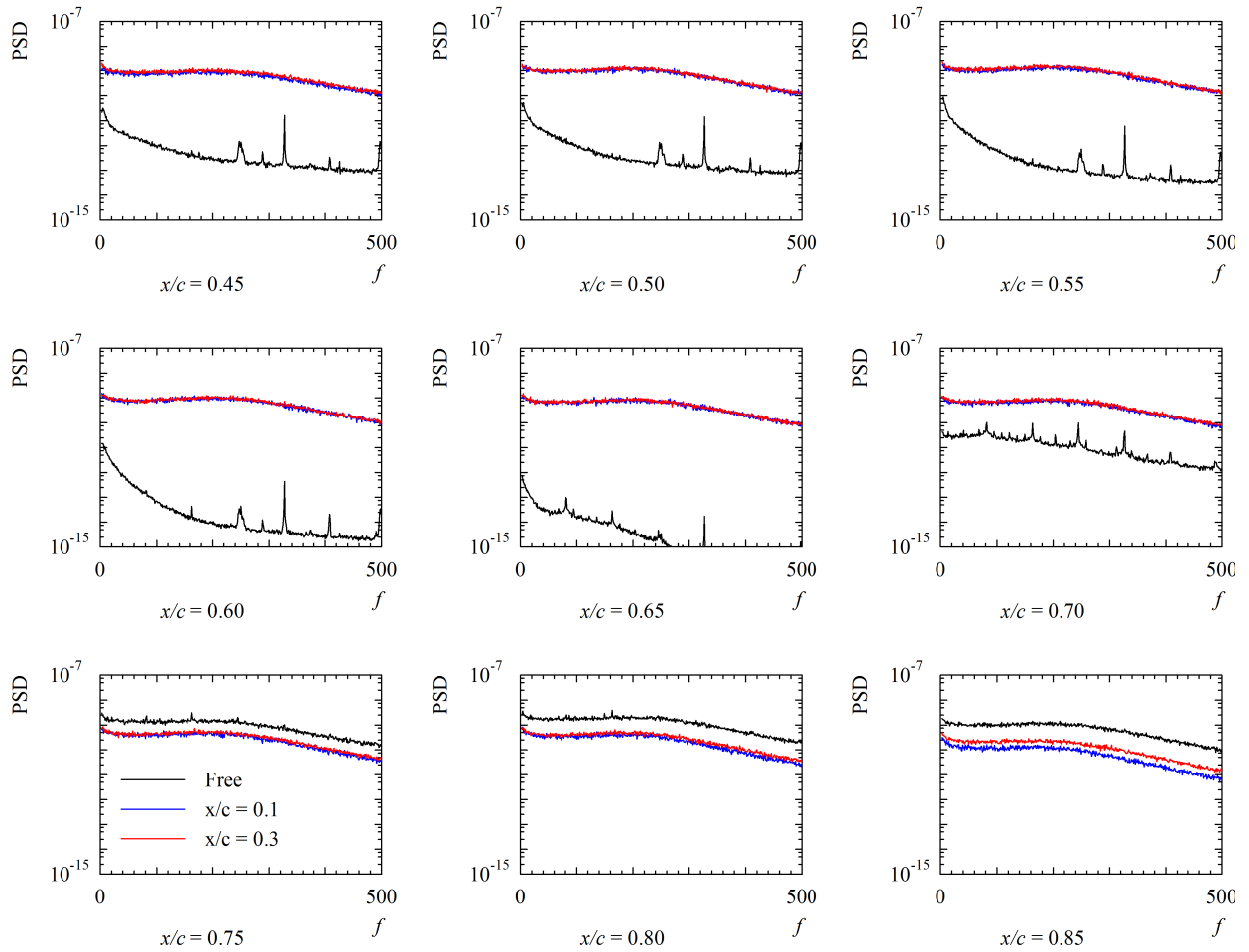


**Fig. 6** PSD of quasi-wall-shear stress for free- and forced-transition cases at  $\alpha = 0^\circ$  ( $Re_c = 6 \times 10^5$ )

forced-transition cases.

For all tested incidences, as the flow moves downstream the shear stress decreases, showing the kinetic energy (momentum) loss in the flow, and CV increases, showing that turbulence is increasing. Whilst free turbulent flows tend to dissipate without a constant energy source, the adverse pressure gradient produces instabilities that lead to turbulence production. As the magnitude of shear stress is representative of the skin friction drag of the wing, it can be observed that the forced-transition cases will likely produce more drag than the free-transition case. As only a small portion of the wing is observed, however, it cannot be concluded how the trip location affects the total drag force. As stated, the decreasing shear stress for the forced-transition cases shows the energy loss in the boundary layer, but as the entire suction surface is not measured the peak shear stress is not

observed. As incidence is increased the difference between the two tested trip locations becomes larger, showing that the influence of forced transition becomes more prominent as the downforce level is increased. Once the shear stress becomes zero near to the trailing edge, as is observed for the  $x/c = 0.1$  trip at  $\alpha = 3^\circ$ , and  $\alpha = 5^\circ$ , the flow has insufficient energy to overcome the adverse pressure gradient and is separated. As the flow-visualisation tests showed, trailing-edge separation occurred in all forced-transition tests, however, for some cases this occurred downstream of the last gauge location.

Understanding of the boundary-layer state and energy content is given by the PSD of the quasi-wall-shear stress in Fig. 6 at zero incidence. In the free-transition case for the upstream gauges, where the boundary layer is laminar, the energy is relatively small and contained in the lower frequency range. The spikes observed in these first few gauges are noise, however at  $0.65 \leq x/c \leq 0.75$  frequency spikes are observed that are physical phenomena of the flow as it transitions from a laminar to turbulent state. These spikes are first observed at the same point where the coefficient of variation indicates that turbulence production has begun, and thus contributes to the conjecture that these are attributable to transitional phenomena. Once the boundary layer has reattached, at  $x/c \approx 0.75$  the energy is contained across a much broader range of frequencies and the total energy content is much higher than that observed at the gauges located in the laminar boundary layer.

For the forced-transition cases the PSD for all gauges appears similar until close to the trailing edge. The free- and forced-transition results display similar characteristics in terms of energy content across the spectrum for  $x/c \geq 0.8$ . This shows that a truly turbulent boundary layer was produced by the roughness-type trips that were employed.

#### **D. LDA**

Wake surveys were taken at incidences  $\alpha = 0^\circ$ ,  $\alpha = 3^\circ$ , and  $\alpha = 5^\circ$ . The same trends were observed for each case, so the results for only  $\alpha = 0^\circ$  are given here in Fig. 7. As flow moves downstream turbulent mixing causes a thicker wake and the velocity deficit is reduced. The upwash behind the wing, a consequence of the downforce produced by the wing, leads to the wake moving upwards as it moves downstream.

For the forced-transition cases the velocity deficit is increased and the height of the wake cen-



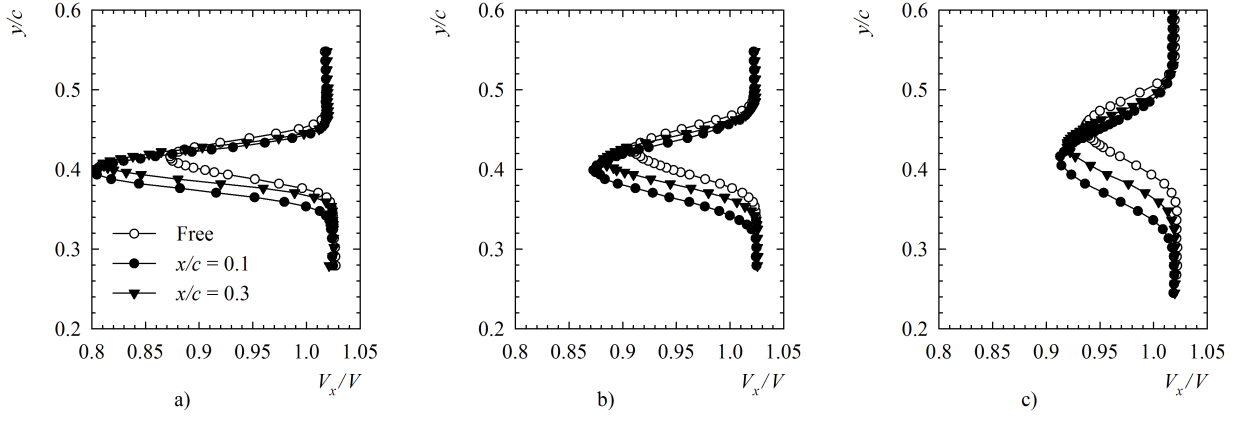


**Fig. 7** Wake surveys for free- and forced-transition cases at  $\alpha = 0^\circ$  for a)  $x/c = 1.5$ , b)  $x/c = 2$ , and c)  $x/c = 3$  ( $Re_c = 6 \times 10^5$ )

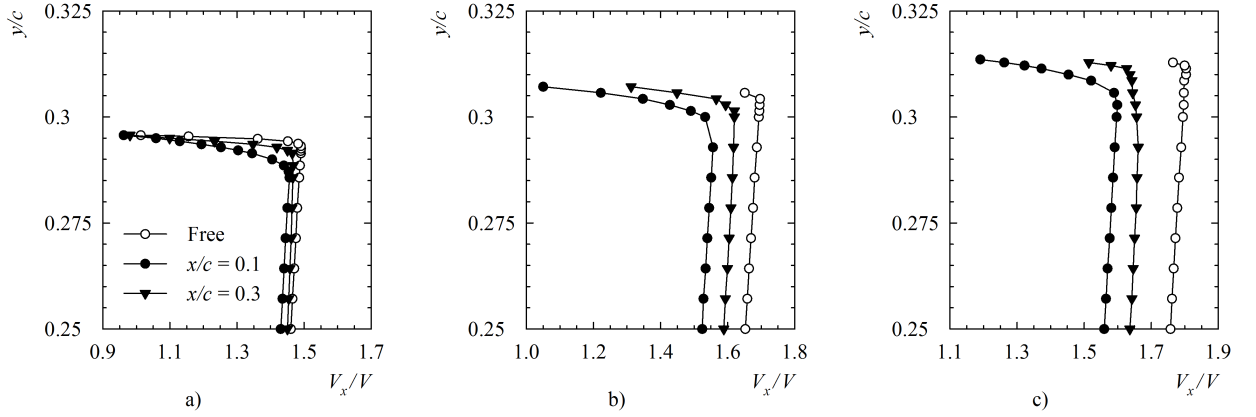


**Fig. 8** Surveys for free- and forced-transition cases at  $x/c = 0.375$  for a)  $\alpha = 0^\circ$ , b)  $\alpha = 3^\circ$ , and c)  $\alpha = 5^\circ$  ( $Re_c = 6 \times 10^5$ )

treline reduced. The area bounded by the velocity deficit is representative of the drag force on the wing. It was suggested in the previous section that the skin friction drag of the wing had increased when forced transition was conducted, it can also be observed by the greater velocity deficit and thicker wake that the total drag has increased. The  $x/c = 0.1$  case, therefore, exhibits the largest drag, followed by the  $x/c = 0.3$  case, and the free-transition case the least. The thicker wake is a result of the trailing-edge separation that was observed in the flow visualisation and thicker boundary layer that occurs in the forced-transition cases, hence the  $x/c = 0.1$  case shows a thicker wake than the  $x/c = 0.3$  case, and both significantly thicker than the free-transition case.

Table 1 shows that the  $x/c = 1.5$  survey shows the largest difference, in terms of area bounded

**Table 1 Percentage difference in the total area bounded by the velocity deficit between the forced-transition cases and the free-transition case**

Forced-Transition		$\Delta W_A$	
Trip Location	$x/c = 1.5$	$x/c = 2$	$x/c = 3$
$x/c = 0.1$	68.4 %	47.1 %	42.0 %
$x/c = 0.3$	54.0 %	28.7 %	18.9 %

by the velocity deficit, between the free- and forced-transition cases; the difference between them steadily reduces as the flow moves downstream. In free-transition, the location of maximum velocity deficit moved upwards from  $y/c = 0.416$  at  $x/c = 1.5$ , to  $y/c = 0.442$  at  $x/c = 3$ ; as a result of the upwash due to circulation. For the  $x/c = 0.1$  trip, however, the reduced downforce generation results in the location of maximum velocity deficit occurring at  $y/c = 0.396$  at  $x/c = 0.15$  and at  $y/c = 0.415$  at  $x/c = 3$ .

The surveys taken underneath the wing at  $x/c = 0.375$  are given in Fig. 8. For all tested incidences the normalised velocity is reduced for the forced-transition cases, where the  $x/c = 0.1$  trip case exhibits the lowest velocity. This is in line with the static pressure measurements as a lower velocity underneath the wing corresponds to a higher pressure (less suction). As incidence is increased, the difference in velocity between the free- and forced-transition cases also increases. It can also be observed that the forced-transition cases exhibit a thicker boundary layer than the free-transition case. By nature the turbulent boundary-layer state is thicker than the laminar counterpart, hence by forcing the turbulent boundary layer to start earlier the boundary layer is thicker. For example, at  $\alpha = 0^\circ$  the difference in thickness between the  $x/c = 0.1$  forced-transition case and the free-transition case can be observed to be  $y/c \approx 0.007$  (2.37%) .

#### IV. Conclusion

The present study investigated the influence of the laminar boundary layer on both the on- and off-surface aerodynamic characteristics of a wing operating in ground effect. This was achieved by using roughness-type boundary-layer trips to force the boundary layer into a turbulent state at specific chord-wise locations. The overall effect of forcing transition was that the laminar separation bubble was eliminated, and trailing-edge separation was shown to occur; this led to a

reduction in downforce and increase in drag. The reduction in downforce was shown by the lower velocity underneath the wing, lower suction on the ground-facing surface and less upwash in the wake, whilst the increase in drag was noted from higher surface-shear stress, a thicker wake, and greater velocity deficit in the wake. It was also shown that each of these aspects was amplified as the trip location, and thus start of the turbulent boundary layer, was moved upstream. This was attributed to the momentum loss in the turbulent boundary layer causing the boundary layer to separate earlier.

The roughness-type trips, formed from double-sided tape and Grit-60 sand, were capable of producing a turbulent boundary layer almost identical, in terms of where in the frequency range energy was contained, to that which formed post-transition in the free-transition case. The downside of the trips, however, was that they were observed to alter the surface pressure immediately before and after the trip.

The results highlight the dramatic effect that laminar boundary layers have on the aerodynamic characteristics of a wing operating in ground effect at Reynolds numbers relevant to practical applications. The majority of computational work into wings in ground effect has utilised fully-turbulent closure models, which, based on the observations in this work, will underestimate aerodynamic efficiency and also, somewhat more importantly, give wake characteristics that are dramatically different. As the front wing of a racing car must condition the flow into a state favourable for downstream components to operate in, modelling the wake is extremely important. It has also been demonstrated that at a full-scale Reynolds number, at which this study was conducted, a laminar separation bubble is still a significant aspect. This highlights that the presented free-transition results are directly applicable to full-scale applications.

Forcing transition is usually used in order to move the transition point upstream to match that of higher Reynolds number flows, however, it is arguable that this is not required as it produces significantly different characteristics to the free-transition case such that the results would be worse than simply allowing the typical Reynolds number scaling effects of a larger bubble of greater aspect ratio to occur.

Through the use of a model of approximately 150% scale at a sub-scale wind speed, a wing in

ground effect has been tested at a Reynolds number equivalent to that which it would operate at on a racing car or light aircraft tailplane. It has been shown that the presence of laminar boundary layers are not only significant, but also their influence on the wing is considerable in almost every aspect. By examining wings where transition was forced at varying locations it was observed that even having the turbulent boundary layer begin at  $x/c = 0.3$  rather than  $x/c = 0.1$  was enough to considerably alter the performance of the wing. Whilst the geometry of the GA(W)-1 aerofoil that was used in this study may have contributed to the dramatic differences observed between free- and forced-transition cases, as it is an aft-loaded profile, based on the presented results it is recommended that any further studies into wings in ground effect, be they experimental or computational, consider the importance of laminar boundary layers.

#### Acknowledgments

Luke Roberts is supported by a Cranfield Defence and Security research bursary.

#### References

- [1] C. Wieselsberger, Wing Resistance Near the Ground, NACA TM 77, 1922.
- [2] E. G. Reid, A Full-Scale Investigation of Ground Effect, Langley Memorial Aero. Lab. Report No. 265, 1926.
- [3] E. A. Stalker, A Reflection Plate Representing the Ground, J. Aero. Sci., vol. 1, no. 3, pp. 151-152 1934.
- [4] I. Tani, M. Taima and S. Simidu, The Effect of Ground on the Aerodynamic Characteristics of a Monoplane Wing, Report No. 156, Aero. Res. Inst., Tokyo Imperial University, 1937.
- [5] J. A. Bagley, The Pressure Distribution on Two-Dimensional Wings near the Ground, RAE Report No. 3238, 1960.
- [6] M. P. Fink and J. L. Lastinger, Aerodynamic Characteristics of Low-Aspect-Ratio Wings in Close Proximity to the Ground, NASA TN D-926, 1961.
- [7] A. Carter, Effect of Ground Proximity on Aerodynamic Characteristics of Aspect Ratio 1 Aerofoils With and Without Endplates, NASA TN D-970, 1961.
- [8] G. H. Saunders, Aerodynamic Characteristics of Wings in Ground Proximity (Ground Effect on Aerodynamic Characteristics of Wings and Lifting Surface Theory for Finite Wing of Arbitrary Planform),

- Canadian Aero. & Space J., vol. 11, pp.185-192, 1965.
- [9] A. J. Berry, An Experimental Investigation of Ground Effect Using a Moving Surface Simulation, MPhil. Thesis, University of London, 1968.
- [10] K. Knowles, D. T. Donogue and M. V. Finnis, A Study of Wings in Ground Effect, RAeS Vehicle Aerodynamics Conference, Loughborough, UK, 1994.
- [11] R. Ranzenbach and J. B. Barlow, Cambered Airfoil in Ground Effect - Wind Tunnel and Road Conditions, AIAA paper no. 95-1909, 1995.
- [12] R. Ranzenbach and J. B. Barlow, Cambered Airfoil in Ground Effect: An Experimental and Computational Study, SAE Paper 96-0909, 1996.
- [13] J. Zerihan and X. Zhang, Aerodynamics of a Single-Element Wing in Ground Effect, Journal of Aircraft, vol. 37, no. 6, pp. 1058-1064, 2000.
- [14] X. Zhang and J. Zerihan, Off-Surface Aerodynamic Measurements of a Wing in Ground Effect, Journal of Aircraft, vol. 40, no. 4, pp. 716-725, 2003.
- [15] J. Correia, L. S. Roberts, M. V. Finnis and K. Knowles, Scale Effects on a Single-Element Inverted Wing in Ground Effect. The Aeronautical Journal, vol. 118, no. 7, pp. 797-809, 2014
- [16] J. Keogh, G. Doig and S. Diasinos, Flow Compressibility Effects Around an Open-Wheel Racing Car, The Aeronautical Journal, vol. 118, no. 1210, pp. 1409-1430, 2014.
- [17] J. Keogh, G. Doig, S. Diasinos and T. Barber, The Influence of Cornering on the Vortical Wake Structures of an Inverted Wing, Proceedings of the Institution of Mechanical Engineers, Part D: Journal of Automobile Engineering, vol. 229, no. 13, pp. 1817-1829, 2015.
- [18] J. Zerihan and X. Zhang, A Single Element Wing in Ground Effect; Comparisons of Experiments and Computation, 39th AIAA Aerospace Sciences Meeting and Exhibit, Reno, NV, 2001.
- [19] G. Doig, T. J. Barber and A. J. Neely, The Influence of Compressibility on the Aerodynamics of an Inverted Wing in Ground Effect, Journal of Fluids Engineering, vol. 133, pp. 1-12, 2011.
- [20] K. Knowles and M. V. Finnis, Development of a New Open-jet Wind Tunnel and Rolling Road Facility. 2nd MIRA International Conference on Vehicle Aerodynamics, Coventry, UK, 1998.
- [21] X. F. Zhang, A. Mahallati & S. A. Sjolander, Hot Film Measurements of Boundary Layer Transition, Separation and Reattachment on a Low-Pressure Turbine Airfoil at Low Reynolds Numbers, AIAA Paper 2002-3643, 38th AIAA/ASME/SAE/ASEE Joint Propulsion Conference & Exhibit, Indianapolis, Indiana, 2002.
- [22] M. S. Selig, J. J. Guglielmo, A. P. Broern and P. Giguere, Experiments on Airfoils at Low Reynolds Numbers, 34th Aerospace Sciences Meeting and Exhibit, Reno, NV, USA, 1996.